Pervasive sources of isotopically light zinc in the North Atlantic Ocean

Nolwenn Lemaitre, Gregory F de Souza, Corey Archer, Ruo-Mei Wang, Hélène Planquette, Géraldine Sarthou, Derek Vance

Pervasive sources of isotopically light zinc in the North Atlantic Ocean

Nolwenn Lemaitre*[1], Gregory F. de Souza[1], Corey Archer[1], Ruo-Mei Wang[1,2], Hélène Planquette[3], Géraldine Sarthou[3], Derek Vance[1]

[1] Department of Earth Sciences, Institute of Geochemistry and Petrology, ETH-Zürich, Zürich, Switzerland

[2] Institute of Earth Sciences, Academia Sinica, Taipei, Taiwan

[3] Laboratoire des Sciences de l'Environnement Marin (LEMAR), UMR 6539, IUEM, Technopôle Brest Iroise, 29280 Plouzané, France

*Corresponding author: Nolwenn Lemaitre (nolwenn.lemaitre@erdw.ethz.ch)

Keywords: zinc isotopes, North Atlantic, zinc sources, GEOTRACES, GEOVIDE

Highlights:

- Hydrothermal and sedimentary sources of light $\delta^{66}Zn$
- $\delta^{66}Zn$ and abundance ratios to the major nutrients deconvolve key processes
- Light $\delta^{66}Zn$ in the surface North Atlantic due to Zn addition, not scavenging

Abstract

In this study, we report seawater dissolved zinc (Zn) concentration and isotope composition ($\delta^{66}Zn$) from the GEOTRACES GA01 (GEOVIDE) section in the North Atlantic. Across the transect, three subsets of samples stand out due to their isotopically light signature: those close to the Reykjanes Ridge, those close to the sediments, and those, pervasively, in the upper ocean. Similar to observations at other locations, the hydrothermal vent of the Reykjanes Ridge is responsible for the isotopically light Zn composition of the surrounding waters, with an estimated source $\delta^{66}Zn$ of -0.42‰. This isotopically light Zn is then transported over a distance greater than 1000km from the vent. Sedimentary inputs are also evident all across the trans-Atlantic section, highlighting a much more pervasive process than previously thought. These inputs of isotopically light Zn, ranging from -0.51 to +0.01 ‰, may be caused by diffusion out of Zn-rich pore waters, or by dissolution of sedimentary particles.

The upper North Atlantic is dominated by low $\delta^{66}Zn$, a feature that has been observed in all Zn isotope datasets north of the Southern Ocean. Using macronutrient to Zn ratios to better understand modifications of preformed signatures exported from the Southern Ocean, we suggest that low upper-ocean $\delta^{66}Zn$ results from addition of isotopically light Zn to the upper ocean, and not necessarily from removal of heavy Zn through scavenging. Though the precise source of this isotopically light upper-ocean Zn is not fully resolved, it seems possible that it is anthropogenic in origin. This view of the controls on upper-ocean Zn is fundamentally different from those put forward previously.

1. Introduction

Zinc (Zn) is an essential micronutrient for marine primary producers (Morel and Price, 2003). It is required for key metalloenzymes such as carbonic anhydrase, which is involved in carbon fixation, or alkaline phosphatase, which gives phytoplankton access to organic forms of phosphorus when phosphate concentrations are low (Sunda, 1989). As a result, the marine cycles of zinc and carbon are intrinsically linked.

Analytical advances over the last decade have enabled study of the stable isotope composition of Zn ($\delta^{66}Zn$ = variations in $^{66}Zn/^{64}Zn$ expressed in parts per thousand deviation from the JMC Lyon standard), to investigate the processes controlling the marine Zn distribution (Bermin et al., 2006; Conway et al., 2013; Takano et al., 2013). In addition, the recent international programme GEOTRACES has provided a large quantity of high-quality data, from full-depth profiles and sections, allowing new insights into the large-scale distribution of trace elements, including Zn (Conway and John, 2014, 2015; Zhao et al., 2014; Vance et al., 2016; John et al., 2018; Weber et al., 2018; Wang et al., 2019). However, gaps remain in our understanding of the modern Zn cycle. Firstly, the $\delta^{66}Zn$ of seawater (averaging +0.46 ‰) is higher than the known inputs and lower than most known outputs, pointing to a missing budget term if the oceanic Zn cycle is in steady state (Little et al., 2014; Moynier et al., 2017). Secondly, north of the Southern Ocean, a shift toward light Zn isotope signatures in the dissolved pool is observed within the upper ocean (<1000m). This is surprising, given that isotopic fractionation between phytoplankton cells and the dissolved pool is thought to be close to zero, or slightly in favour of light isotope uptake, which should leave the residual dissolved pool slightly heavy (John et al., 2007; Peel et al., 2009; Samanta et al., 2017; Köbberich and Vance, 2019; Wang et al., 2019). Laboratory experiments have suggested that Zn released from degrading phytoplankton cells can

71 be rapidly scavenged back onto organic matter, and that this adsorbed Zn is
72 isotopically heavier than the dissolved pool (John and Conway, 2014). Scavenging of
73 isotopically heavy Zn onto sinking biogenic particles has thus been suggested to
74 explain the low δ^{66}Zn values in the upper ocean (Conway and John, 2014, 2015; John
75 et al., 2018; Weber et al., 2018), although it should be noted that a dominant proportion
76 of marine dissolved Zn is complexed to natural organic ligands (e.g. Ellwood and Van
77 den Berg, 2000) and thus presumably not available for adsorption to particles.

78 Here we examine Zn isotopes and concentrations along a GEOTRACES section that
79 crosses the North Atlantic from the Iberian Peninsula to Newfoundland (Fig. 1). The
80 North Atlantic is a promising area to study biological, physical and geochemical
81 processes affecting micronutrient distributions, as it is characterised by a strong spring
82 bloom (Longhurst, 2010), the formation of globally-important deep water masses (e.g.
83 Daniault et al., 2016), and a variety of trace metal sources (Ohnemus and Lam, 2014).
84 In this study, we focus our discussion on the processes responsible for the light isotope
85 composition of Zn observed at the Reykjanes Ridge, at the sediment-water interface,
86 and in the upper 500m of the ocean. In doing so, we expand our analysis to data from
87 the entire North Atlantic. We combine macronutrient/Zn ratios with Zn stable isotope
88 data for the dissolved pool in order to better identify the processes that modify
89 preformed Southern Ocean signatures in the low-latitude oceans. In contrast to
90 previous studies that invoke scavenging removal of heavy Zn isotopes for the origin of
91 light upper-ocean Zn (e.g. John and Conway, 2014), we conclude that the Zn isotope
92 signature of the upper ocean is dominated by the addition of isotopically light Zn to
93 upper-ocean water masses, whose preformed Zn concentrations are extremely low
94 (Vance et al., 2017; de Souza et al., 2018; Middag et al., 2019), and which are thus
95 very sensitive to the addition of small amounts of Zn.

2. Methods

2.1. Study area and sample collection

Samples were collected during the GEOVIDE cruise (GEOTRACES GA01) from 15 May to 30 June 2014 (R/V Pourquoi Pas?). At six stations, 17 depths between the surface and the seafloor were sampled for dissolved Zn concentrations and stable isotope composition (expressed as $\delta^{66}Zn$; see Eq. 1 below). These 6 stations (Fig. 1) are located within the Iberian basin (Station 13), the west European basin (Station 21), the Icelandic basin (Stations 32 and 38) with Station 38 just above the Reykjanes Ridge, the Irminger basin (Station 44) and the Labrador basin (Station 69).

Samples were collected using a clean rosette equipped with cleaned 12 litre GO-FLO bottles, following the recommendations of the GEOTRACES cookbook (Cutter et al., 2017). After recovery, the bottles were transferred into a clean container and seawater samples were filtered through 0.45 µm polyethersulfone filters (Pall, Supor^{TM}) mounted in Swinnex polypropylene filter holders (Millipore). Between 1 and 4 litres of filtrate were collected into acid-cleaned polyethylene bottles. More details of the sampling procedure can be found in Gourain et al. (2019).

2.2. Sample processing and analysis

At ETH Zürich, samples were acidified to pH ~2 by addition of concentrated hydrochloric acid (HCl; Merck AnalaR grade, further purified by double sub-boiling distillation) and left for at least 1 month before processing. All samples were processed under clean laboratory conditions in clean hoods, using only trace metal clean Savillex PFA labware. All water used was ultrapure (≥18.2 MΩ.cm) and all acids and reagents were Merck AnalaR grade, further purified by single or double sub-boiling distillation.

Samples were first doped with a ^{67}Zn-^{64}Zn double spike to achieve a sample:spike ratio of ~1. After 48 hours of equilibration, an ammonium acetate buffer solution was added and pH was increased to 5.0 ± 0.3. Zinc was extracted from seawater with Nobias PA1 resin and purified using AGMP-1 anion exchange resin (Bermin et al., 2006; Takano et al., 2013; Vance et al., 2016). Total procedural blanks were assessed by processing ultrapure water as a sample, and were 1.8 ± 0.6 ng, with a $\delta^{66}Zn$ of +0.46 ± 0.28 ‰ (average and 2SD, n=8). Blank contributions were barely significant (mostly involving a correction of 0.01-0.02 ‰) for all except three samples: Station 13-15m (0.10 ‰ shift), Station 21-50m (0.08 ‰ shift) and Station 44-159m, (0.12 ‰ shift). Nonetheless, Table S1 gives blank-corrected data with propagated uncertainty in the blank amount and isotope composition.

Isotopic analyses were performed at ETH Zürich using a Thermo-Finnigan Neptune Plus multi-collector inductively-coupled-plasma mass spectrometer (MC-ICPMS) in 'low-resolution' mode. Samples were introduced in 1 mL 0.3M nitric acid (HNO_3) via a CPI PFA nebulizer (50 $\mu L.min^{-1}$) attached to an Aridus II desolvating system. Dissolved Zn concentrations were obtained by isotope dilution. Analytical mass bias correction was performed using the double spike technique (Bermin et al., 2006). Dissolved Zn isotope compositions ($\delta^{66}Zn$) were calculated following the iterative approach of Siebert et al. (2001) and are given in the standard delta per mil notation relative to the JMC-Lyon standard:

$$\delta^{66}Zn\ (‰) = \left[\frac{\left(\frac{^{66}Zn}{^{64}Zn}\right)_{\text{sample}}}{\left(\frac{^{66}Zn}{^{64}Zn}\right)_{\text{JMC Lyon}}} - 1\right] \times 1000 \qquad (1)$$

During the course of this study, and owing to the exhaustion of the existing JMC-Lyon stock, Zn data were normalised to a new primary standard, AA-ETH Zn. Where this

was the case, data were converted to the JMC-Lyon delta scale by applying a conversion factor of -0.28 ‰ (Archer et al., 2017). Long-term reproducibility of Zn isotope analysis on the instrument is monitored by repeat analysis of a secondary standard, IRMM-3702, which yields $\delta^{66}Zn$ = +0.30 ± 0.06 ‰, relative to JMC-Lyon, over 5 years (n = 543, 2SD). Internal errors obtained from the mass spectrometry analysis, propagated through the double spike calculations and including the uncertainty arising from the blank correction, were generally lower than the long-term reproducibility. These internal uncertainties are given in the data table. Uncertainties plotted on the figures are the internal uncertainties or the long-term reproducibility, whichever is the larger. Zinc isotope reproducibility for samples, as assessed by full analytical replicates of 14 samples, was consistent with long-term standard reproducibility. Differences between these replicates ranged between 0.00 and 0.14 ‰ and averaged 0.05 ± 0.04 ‰. This laboratory has demonstrated agreement for Zn concentrations and isotopes with the GEOTRACES standards SAFe D1 and D2 using similar methods in a number of past papers (Zhao et al., 2014; Sieber et al., 2020) and with the GEOTRACES intermediate data product (IDP 2017; Schlitzer et al., 2018). Furthermore, analyses of deep ocean samples yield the same results as obtained in other studies (e.g. Conway and John, 2014; Sieber et al., 2020; Vance et al., 2016; Wang et al., 2019).

2.3. Other oceanographic parameters

Concentrations of the macronutrients silicate (Si) and nitrate (NO_3^-) were obtained by the nutrient group at the LEMAR laboratory, using the method described in Aminot and Kérouel (2007). Because of technical problems, phosphate data are not available. Hydrographic parameters (oxygen, salinity, temperature) were used to define the

water mass distribution and the general circulation along the GEOVIDE transect, as described by García-Ibáñez et al. (2018).

2.4. Dissolved Zn*

Since the first reliable Zn data (Bruland, 1980), and further confirmed by the efforts of the GEOTRACES programme to produce high-resolution Zn data (Schlitzer et al., 2018), a strong correlation is observed between Zn and Si concentrations throughout the global ocean (Vance et al., 2017; de Souza et al., 2018). Any variability in this relationship highlights either sources or sinks of Zn relative to Si, such as biological uptake or regeneration of Zn and Si at different rates, or an addition to or loss from the water column (Wyatt et al., 2014; Roshan and Wu, 2015; Kim et al., 2017). To illustrate deviations from the global marine Zn-Si correlation, we use the Zn* parameter, which is defined as:

$$Zn^* = [Zn]_{measured} - \left(Zn/Si_{deep} \times [Si]_{measured}\right) \quad (2)$$

with Zn/Si_{deep} set at 0.06 mmol.mol^{-1}, representing the average Zn/Si ratios in the global deep ocean. Note that the average Zn/Si ratios across the GEOVIDE transect for depths ≥3000m (excluding the deepest samples, closest to the sediment-water interface, in each depth profile; see section 4.2) is 0.08 mmol.mol^{-1}.

3. Results

Dissolved Zn concentrations vary from 0.07 to 5.95 nmol.L^{-1}, δ^{66}Zn values from -0.22 to +0.53 ‰, and Zn* from -0.25 to +5.29 nmol.L^{-1} across the entire GEOVIDE section (Fig. 2 and 3; Table S1). Dissolved Zn concentrations exhibit a typical nutrient-type profile, with low concentrations throughout the surface ocean (<0.50 nmol.L^{-1} in the

upper 20m, except at Station 32 where it reaches 1.00 nmol.L^{-1} at 30m) and an increase with depth, reaching up to 5.95 nmol.L^{-1} close to the Reykjanes Ridge.

Zn* values in the upper ocean are close to zero, even if slightly positive (+0.08 ± 0.30 nmol.L^{-1}, n=9, median ± 1SD), and increase with depth, reaching maximum values close to the sea floor. The picture in the deep eastern part of the section (Iberian and west European basins) is slightly more complex, with a mid-depth maximum in Zn* values overlying lower values between 2000 and 5000m. Overall, Zn* values are positive, indicating an enrichment of Zn relative to Si. This general Zn enrichment is also indicated by the greater Zn/Si_{deep} ratio of the North Atlantic along GEOVIDE (0.08±0.03 mmol.mol^{-1}) compared to the world ocean (0.06±0.02 mmol.mol^{-1}; Schlitzer et al., 2018).

The deep ocean (>1500m) across the GEOVIDE transect averages +0.38 ± 0.07 ‰ (average ± 1SD, n=27) in $\delta^{66}Zn$, which is nominally lighter than, but within error of, the global average deep ocean $\delta^{66}Zn$ value (+0.46 ± 0.13 ‰; 2SD, n = 312, 2SE = 0.01 ‰; Schlitzer et al., 2018). Apart from this, three zones stand out from the rest of the section: the upper ocean (between the surface and ~1000m), the area close to the Reykjanes Ridge, and the sediment-water interface (Fig. 2). All are characterised by light Zn signatures, with median $\delta^{66}Zn$ values of -0.13 ± 0.07 ‰ for the upper ocean (n=8), -0.01 ± 0.07 ‰ around the Reykjanes Ridge (n=4), and +0.12 ± 0.16 ‰ for the sediment-water interface (n=5), but they are associated with either high Zn concentrations (close to the Reykjanes Ridge and the bottom) or low Zn concentrations (upper ocean).

4. Discussion

Apart from the marked maximum extending eastwards from the Reykjanes Ridge, the distribution of Zn (Fig. 2) along the GEOVIDE transect bears a strong resemblance to those of the major nutrients (cf. García-Ibáñez et al., 2018), and especially that of Si, reflected by the close correlation between their concentrations that is typical for the open ocean (Fig. 4; Bruland, 1980; Vance et al., 2017; de Souza et al., 2018; Weber et al., 2018). To first order, the cross-basin distributions of Zn, Si and other macronutrients are largely governed by the properties of the water masses found along the transect: water masses formed in the North Atlantic and Nordic Seas are macronutrient- and Zn-poor, and fill the basins west of the Reykjanes Ridge as well as the mid-depths across the entire transect, whereas macronutrient- and Zn-rich waters of southern origin fill the abyss east of the ridge, below about 3000 m (e.g. García-Ibañez et al., 2018). However, despite this first-order water mass control on the elemental distributions of Zn and Si, and in marked contrast to the silicon stable isotope distribution along GEOVIDE (Sutton et al., 2018), the δ^{66}Zn distribution (Fig. 2) displays little systematic cross-basin variation. What stands out instead are the low δ^{66}Zn values at mid-depths, near the bottom, and in the upper ocean. In the following, we discuss each of these in turn.

4.1. Light Zn isotope signatures in the vicinity of the Reykjanes Ridge

Elevated Zn concentrations (5.95 nmol.L^{-1}), high Zn* (up to +5 nmol.L^{-1}) and light δ^{66}Zn values (-0.22 ‰) were determined at Station 38, just above the Reykjanes Ridge (Figs. 2 and 3), suggesting the input of hydrothermally-sourced Zn here. Interestingly, high

Zn concentrations (>2.40 nmol.L^{-1}), again associated with high Zn* (>+1.7 nmol.L^{-1}) and light δ^{66}Zn values (<+0.02 ‰), were also observed between 1500 and 2000m within the Icelandic and west European basins to the east of the ridge (Stations 32 and 21, respectively). Data across this mid-depth Zn maximum from all three stations exhibit a strong positive correlation between δ^{66}Zn and 1/[Zn] (Fig. 5a), suggesting that the "plume" of elevated Zn above and to the east of the Reykjanes Ridge can be explained by mixing between two components: ambient deep seawater and a hydrothermal source. Indeed, hydrothermal vents along the Reykjanes Ridge have been shown to act as a source of other dissolved trace elements, such as iron and manganese (Achterberg et al., 2018). Although their origin could not be definitively determined, it has also been suggested that the enrichments in particulate and dissolved iron and aluminium concentrations observed above Reykjanes Ridge during GEOVIDE (Gourain et al., 2019; Tonnard et al., 2020), as well as the elevated radium-226 activity seen there (Le Roy et al., 2018), may also reflect the influence of hydrothermal activity.

To assess the δ^{66}Zn value of the hydrothermal end-member, we compare Zn concentrations and isotopes observed within the hydrothermal plume at Station 38 with those of background deep seawater from surrounding stations (Station 32: 990-1235m and 2463-3177m; Station 44: 1087-2851m; $[Zn]_{background}$ = 1.46 ± 0.22 nmol.L^{-1} and $\delta^{66}Zn_{background}$ = +0.42 ± 0.06 ‰; median values; n=12). The quantity of hydrothermally-sourced Zn at any depth is estimated by subtracting this background concentration from the measured concentration at this depth. The strong linear correlation between δ^{66}Zn and the fraction of hydrothermally-derived Zn (calculated by dividing the estimated quantity of hydrothermal Zn by the total Zn concentration) suggests that the hydrothermal end-member bears a δ^{66}Zn value of -0.42 ± 0.11 ‰

(Fig. 5b). This value is very similar to the hydrothermal $\delta^{66}Zn$ signature of -0.5 ‰ estimated for the TAG hydrothermal field at 26°N in the North Atlantic (Conway and John, 2014). The total range of $\delta^{66}Zn$ in pure hydrothermal fluids, from 0.00 to +1.33 ‰ (John et al., 2008), with recent inferred values of +0.24 ‰ at the East Pacific Rise (John et al., 2018), suggest that the hydrothermal $\delta^{66}Zn$ signature likely depends on the ridge characteristics.

The low $\delta^{66}Zn$ observed at Stations 32 and 21 is likely the result of transport by Labrador Sea Water (LSW; Fig. 1), which crosses the Mid-Atlantic Ridge (MAR) at latitudes around 50°N and spreads eastward into the Icelandic and west European basins (e.g. Paillet et al., 1998; Sutton et al., 2018). The hydrothermal signal, acquired when crossing the MAR, thus seems to propagate over a distance of 1000km (from the MAR to Station 21). This is in contrast to the observations of Conway and John (2014) who did not find any extension of the Zn hydrothermal signal away from the MAR along their east-west section, likely because of the north-south deep water mass circulation there (Jenkins et al., 2015). Our results are, however, similar to other studies that have reported long-distance transport of hydrothermally-derived Zn along with the deep water mass flow direction (Wheat et al., 2002; Roshan et al., 2016; John et al., 2018). The light hydrothermal $\delta^{66}Zn$ signature may be transported as nanoparticulate sulphide species (Conway and John, 2014; John et al., 2018), since sulphide is known to preferentially sequester light Zn (Archer et al., 2004; Fujii et al., 2011; Vance et al., 2016).

4.2. Light Zn isotope signatures at the sediment-water interface

A striking feature all across the transect is the sharp increase in Zn concentrations and Zn* at the very bottom of each profile (up to 4.02 nmol.L^{-1} and +2.5 nmol.L^{-1}, respectively; Fig. 3), associated with a shift to lighter δ^{66}Zn signatures (as low as -0.16 ‰). Importantly, this shift consistently occurs between the deepest sample and the one immediately above it, i.e. over a depth interval of 25 to 425m. The mirror image between δ^{66}Zn and Zn* profiles suggests the addition of isotopically light Zn to seawater close to the seafloor.

The fact that we observe isotopically-light sedimentary Zn input all across the transect is surprising compared to the findings of previous studies, in which such isotopic signals were observed only near margin sediments in the subtropical North Atlantic (from -0.7 to -0.5 ‰; Conway and John, 2014) and the California basin (-0.3 ‰; Conway and John, 2015). Since all our near-bottom samples were taken from the same GO-FLO bottle (in rosette position 1), we must consider the possibility of contamination. Zurbrick et al. (2018) observed a decrease of the excess lead (Pb) concentration in this bottle (i.e. the difference in Pb concentrations between the near-bottom sample and its nearest neighbour) as the GEOVIDE cruise proceeded, pointing to a wash-out of Pb contamination from the GO-FLO bottle with time. However, we observe no decrease of excess Zn over time (Fig. S1). Furthermore, unlike Zn, Pb concentrations are very low in the deep North Atlantic due to its different geochemical behaviour (~0.02 nmol Pb.L^{-1} compared to ~2.0 nmol Zn.L^{-1}), such that Pb is much more prone to contamination in deep-water samples than Zn. Therefore, we suggest that these near-bottom samples reflect true ocean Zn signals that document a sedimentary source of Zn.

On the GEOVIDE cruise, the deepest sample was taken at 4-32m (15m on average) above the seafloor. This is in contrast to the subtropical North Atlantic section, along which the light signal at the bottom was only found at the continental margins, where the deepest samples came from between 33 and 299m above the seafloor (76m on average; Conway and John, 2014). This greater difference from the seafloor could explain why the sedimentary input was not observed across the entire transect by Conway and John (2014), and would suggest that the light sediment-derived $\delta^{66}Zn$ signal does not persist far from the seafloor.

By comparing the deepest Zn concentration and $\delta^{66}Zn$ value with those of the deep seawater background at each station, the $\delta^{66}Zn$ value of the local sedimentary source (Table S2) can be deduced from mass balance. This calculation results in different sedimentary Zn isotope signatures for the eastern (Iberian and west European basins) and western (Icelandic, Irminger and Labrador basins) sections of the transect, with $\delta^{66}Zn$ values of 0.01 ± 0.02 ‰ and -0.51 ± 0.04 ‰ respectively (Table S2). This variation might be explained by different types of sediment, or different processes releasing Zn to seawater, on either side of the sub-arctic front (SAF; Fig. 1).

The processes that might provide light Zn to the bottom waters are not constrained by our data. However, upward diffusion from Zn-rich pore waters is consistent with ^{226}Ra enrichments close to the seafloor (Le Roy et al., 2018) in the eastern basin. In the western basin, dissolution of sedimentary particles might be the important process controlling the Zn source, as Gourain et al. (2019) observed high particulate iron, manganese and aluminium concentrations associated with low beam transmissometry values, suggesting sediment resuspension. Release of biogenic Zn from the sediments or dissolution of Zn sulphides could also explain the near-bottom isotopically light Zn signatures (Conway and John, 2014, 2015). Regardless of the

precise process of addition, the extension of this near-bottom feature all the way across the GEOVIDE transect suggests that the addition of isotopically-light zinc from sediments is a much more pervasive process in the ocean than previously thought.

4.3. Light Zn isotope signatures in the upper ocean

Within the upper 500m, low Zn concentrations are observed in our North Atlantic transect (as low as 0.07 nmol.L^{-1}; Fig. 2 and 3) as well as other oceanic regions north of the Southern Ocean (Conway and John, 2014, 2015; John et al., 2018). Zn* values in the GEOVIDE data are close to zero as a result of low Zn and Si concentrations, though 13 out of 14 data points are positive (between -0.21 and +0.87 nmol.L^{-1}; Fig. 3), and δ^{66}Zn values are low (as low as -0.18 ‰). Other studies, in the North Atlantic as well as in the tropical and North Pacific, have noted similarly low δ^{66}Zn values in the upper ocean (Conway and John, 2014, 2015; John et al., 2018; Vance et al., 2019; Liao et al., 2020), which is at odds with the first-order expectation that biological Zn uptake should slightly enrich upper-ocean Zn in its heavy isotopes, given the fractionation observed in culture and deduced for natural freshwater systems (John et al., 2007; Peel et al., 2009; Samanta et al., 2018; Köbberich and Vance, 2019). This finding has led to the hypothesis that isotopically heavy Zn is removed by scavenging, explaining the light δ^{66}Zn values in the upper ocean (Conway and John, 2014, 2015; John et al., 2018; Weber et al., 2018). However, given the strong preformed upper-ocean gradients in Zn concentrations resulting from interactions between biological activity and physical circulation at the large scale, which primarily occur in the Southern Ocean (e.g. Vance et al., 2017), assessing the presence of a small *in-situ* upper-ocean source or sink in the lower latitudes is a significant challenge.

In order to disentangle the signal of local/regional upper-ocean processes from large-scale nutrient cycling, we compare $\delta^{66}Zn$ values and macronutrient/Zn ratios observed across the GEOVIDE section with data from the Southern Ocean (Fig. 6; we use macronutrient/Zn ratios, and not Zn/macronutrient ratios, since binary mixing produces linear relationships between $\delta^{66}Zn$ and 1/Zn). The GEOVIDE isotope profiles, in common with all others north of the Southern Ocean, contrast strongly with the homogeneous isotope profiles observed south of the Antarctic Polar Front (Zhao et al., 2014; Wang et al., 2019; Sieber et al., 2020). Water masses that fill the global ocean transport this homogeneous Southern Ocean $\delta^{66}Zn$ signature northwards, whilst also influencing global distributions of Zn and the macronutrients nitrate (NO_3^-) and Si (Sarmiento et al., 2004; Vance et al., 2017). Southern Ocean waters supplying the upper ocean are stripped of Zn relative to NO_3^- and phosphate, and thus bear high NO_3^-/Zn ratios, whilst abyssal waters carry the equivalent regenerated Zn, and thus bear NO_3^-/Zn ratios 1-2 orders of magnitude lower. Ratios of Si/Zn in the Southern Ocean source waters vary much less than NO_3^-/Zn, by less than factor 2, due to coupled uptake of Zn and Si at the surface by Southern Ocean diatoms (Vance et al., 2017; de Souza et al., 2018). These Southern Ocean water masses are transported northwards globally, including into the northern North Atlantic: abyssal water masses of Southern Ocean origin can be traced as far north as 58°N (e.g. van Aken and Becker, 1996), whilst the upper limb of the meridional overturning circulation transports upper Southern Ocean water masses into the North Atlantic (e.g. Marshall and Speer, 2012) where they influence the biogeochemical characteristics of water masses formed in the North Atlantic and Nordic seas (e.g. (Williams et al., 2006; de Souza et al., 2012, 2015). The isotopic and elemental ratio signatures of Southern Ocean water masses (black rectangles in Fig. 6; Sieber et al., 2020) thus provide the framework

within which we interpret the controls on Zn and its isotopes here: deviations from the Southern Ocean elemental ratio signatures indicate a decoupling of Zn from the macronutrients, which may reflect either differential biogeochemical cycling (e.g. different depths of remineralisation) or the presence of sources or sinks of Zn that do not affect macronutrient concentrations.

As can be seen in Fig. 6, NO_3^-/Zn and Si/Zn in the deepest ocean across GEOVIDE (i.e., in southern-sourced deep waters, depths > 3000m east of the Reykjanes Ridge; empty symbols in Fig. 6) are generally near-identical to the signatures observed in deep Southern Ocean waters. In the intermediate and upper ocean, however, the GEOVIDE data show lower NO_3^-/Zn and Si/Zn ratios than the relevant Southern Ocean source, up to a factor of 260 and 11 respectively. This decoupling between Zn and the macronutrients, with a decrease in macronutrient/Zn ratios, suggests that there is an *addition*, not removal, of Zn relative to NO_3^- and Si, especially in the upper ocean. In the next section, we consider the influence of this relative Zn source on the δ^{66}Zn distribution over the entire North Atlantic.

4.4. Addition of isotopically light Zn: a pervasive process in the North Atlantic

Isotopically light Zn signatures in the upper ocean have also been observed in the subtropical North Atlantic (δ^{66}Zn as low as -0.69 ‰ at 80m, GA03 transect; Conway and John, 2014), as well as in other ocean basins (John et al., 2018). Here, we aim to demonstrate that the low upper-ocean δ^{66}Zn signature observed in the entire North Atlantic (GA03 & GEOVIDE sections; Schlitzer et al., 2018) has a single cause: the addition of isotopically light Zn.

Figure 7 shows the relationship between NO_3^-/Zn (Fig. 7a) or Si/Zn (Fig. 7b) and δ^{66}Zn for all North Atlantic data. These North Atlantic data are compared to the corresponding Southern Ocean signatures (black rectangles), which vary in elemental ratios but not in δ^{66}Zn. Samples from oxygen-rich waters (oxygen saturation > 60%; colour coding in Fig. 7) generally follow trends towards lower δ^{66}Zn values with decreasing NO_3^-/Zn and Si/Zn (black arrows). These trends illustrate the fact that light δ^{66}Zn values are mostly associated with an enrichment in Zn relative to Si or NO_3^- (i.e., lower macronutrient/Zn ratios). This relationship suggests that the North Atlantic δ^{66}Zn distribution is influenced by the addition of isotopically light Zn, similar to the recent inference of an isotopically light external source influencing the δ^{66}Zn distribution of the Northwest Pacific (Liao et al., 2020). In Figure 7, Zn-poor upper-ocean samples, which plot towards the bottom left corner of each plot, tend to be more strongly affected, appearing to have both a stronger *relative* source (at lower macronutrient and Zn concentrations) and lower δ^{66}Zn values. Conversely, samples from oxygen-poor regions (oxygen saturation < 50%) such as at the Mauritanian upwelling regime show an opposite trend, towards higher NO_3^-/Zn and Si/Zn ratios than the Southern Ocean. This depletion of Zn relative to the macronutrients was noted by Conway and John (2014), who attributed it to Zn loss either through sulphide precipitation or scavenging onto particles sinking through the oxygen-poor zone.

Figure 8 shows the correlation between Si and Zn concentrations in the North Atlantic, with data points colour-coded for δ^{66}Zn values. Vertical deviations from the well-known near-linear global Zn-Si relationship (Vance et al., 2017; de Souza et al., 2018; Roshan et al., 2018; Weber et al., 2018) indicate either addition (data above the dotted line) or removal (data below the dotted line) of Zn relative to Si. Even in this simple representation, numerous sources of relative Zn addition are visible in the North

Atlantic data. Hydrothermal and sedimentary addition of Zn relative to Si is seen for the deep ocean (Si concentrations ≥ 10 µmol.L^{-1}), with the associated δ^{66}Zn being variable but relatively low (between -0.2 and +0.3 ‰). However, the cluster of data points above the global relationship at low Si concentrations (< 5 µmol.L^{-1}) is a clear sign of relative excess Zn in the Si-poor shallow ocean. Importantly, these samples are characterised by the lowest δ^{66}Zn values observed in the North Atlantic (between -0.6 and -0.1 ‰).

Taken together, our analysis of the North Atlantic δ^{66}Zn distribution in the large-scale biogeochemical context suggests that addition of isotopically light Zn is the dominant process controlling the upper-ocean Zn isotope signature, at least in the North Atlantic. Macronutrient/Zn depth profiles (Fig. 6) and systematics (Fig. 7 and 8) suggest that this addition may be pervasive over the upper 2000 – 3000m of the water column; this suggests that the addition is most clearly reflected in *upper-ocean* δ^{66}Zn values mainly because preformed Zn concentrations are extremely low there (Middag et al., 2019). In these waters, Zn isotope compositions can be more easily modified by modest Zn inputs compared to Zn-rich deep waters, such that a broadly-distributed source of isotopically light Zn addition would be more easily observed in the Zn-poor upper ocean.

4.5. Potential sources of isotopically light Zn

It is clear from the preceding discussion that different sources contribute to the isotopically light Zn observed throughout the GEOVIDE section. Hydrothermal inputs and sedimentary sources (see Sections 4.1 and 4.2 respectively) have δ^{66}Zn values of around -0.5 ‰. The most important new conclusion here is that the open upper

457 ocean also sees the addition of light Zn. We see two broad mechanisms for the origin
458 of this light Zn.

459 It is possible that the source responsible for the isotopically light Zn in the upper ocean
460 (see Sections 4.3 and 4.4), which bears a similar isotope signature to the hydrothermal
461 and sedimentary sources (Fig. 7), is the same as one of these, transported laterally,
462 and with a much more obvious impact on the open upper ocean because of the low
463 Zn concentrations there. Thus, for example, sedimentary sources of isotopically light
464 Zn observed previously in bottom waters close to the Iberian, North and South
465 American margins (Conway and John, 2014, 2015; John et al., 2018), and here more
466 pervasively at the sediment-water interface, could be transported laterally into the
467 open upper ocean, where its influence may remain visible over greater spatial scales
468 than in the deep ocean due to lower background concentrations. Conway and John
469 (2014) have pointed to the potential role of the Gulf Stream in transporting light surface
470 Zn isotope signatures from the North American coast into the basin. Similarly, currents
471 or water masses may have played a role in transporting the isotopically light Zn across
472 the GEOVIDE transect. For example, an isotopically light Zn signal could be
473 transported from the Caribbean and the American coasts across the North Atlantic,
474 via the North Atlantic Current (NAC; Fig. 1).

475 It is also possible that the light zinc in the upper ocean and close to the sediment-water
476 interface both have their ultimate origin in the upper ocean. For example, particulate
477 material from the atmosphere or from rivers transits the surface ocean on its way to
478 the sediment, potentially releasing labile Zn in the upper ocean and continuing to act
479 as a source from the seafloor over longer timescales. Zinc isotope signatures for rivers
480 and aeolian dust have been reported by Little et al. (2014) and average +0.33 and
481 +0.37 ‰ respectively, values that are similar to the upper continental crust (UCC;

+0.31 ± 0.12 ‰; Moynier et al., 2017). These sources are thus too heavy to explain the isotopically light Zn signature. However, across the GEOVIDE transect, Zn in dust is a mixture of mineral and anthropogenic sources (Shelley et al., 2017), and the anthropogenic component is more important close to the European and American continents (Shelley et al. 2018). Volatile contaminants (smelter dust, fly ash, emissions) tend to have light Zn isotope signatures (from -0.67 to +0.21 ‰; Mattielli et al., 2009; Fekiacova et al., 2015), which are consistent with the light Zn values in the upper 100m (between -0.17 and -0.01 ‰). It is also well known that these anthropogenic components are much more labile than mineral dust (Conway et al., 2019; Desboeufs et al., 2005; Hsu et al., 2005; Shelley et al., 2018). Alternatively, the Tagus river, which drains into the Atlantic ocean near Lisbon, is affected by agriculture and industrial activities; it is known to discharge large quantities of Zn (Le Gall et al., 1999; Cotté-Krief et al., 2000) but, to our knowledge, there are no Zn isotope data available. These riverine contaminants could be transmitted to estuarine sediments, and transported off the coast to transmit their isotope signatures to the dissolved pool after dissolution. In summary, there is at least the potential for both aeolian and riverine sources of anthropogenically-sourced light Zn to the ocean.

5. Conclusion

We have analysed Zn concentrations and stable isotope compositions in the North Atlantic across the GEOVIDE section. The greatest variations in $\delta^{66}Zn$, all associated with isotopically light Zn, are observed close to the Reykjanes Ridge, close to the seafloor and in the upper ocean. Close to the Reykjanes Ridge, the hydrothermal vent releases isotopically light Zn to the ocean that is transported eastwards into the northeast Atlantic. This hydrothermal Zn may not be truly dissolved, but rather

associated with sulphide nanoparticles. We also show that the addition of isotopically light Zn from the sediments is a much more pervasive process in the ocean than previously recognised. Possibly due to higher depth resolution near the sediment-water interface than previous studies, we observed this feature all across the transect, rather than just at the margins. Finally, our analysis of the relationships between macronutrient/Zn ratios and Zn isotopes strongly suggests that the isotopically light Zn signature of the upper ocean is also caused by an addition of Zn to the ocean.

Overall, we put forward a fundamentally different view of upper-ocean Zn and its isotopes than that presented in previous studies, one whose framework for the interpretation of oceanic Zn and its isotopes emphasises preformed Southern Ocean-derived water mass signatures and how they are modified in the low-latitude oceans. If correct, it is the addition of light Zn that explains the low δ^{66}Zn values of the low-latitude upper ocean, and not the removal of heavy isotopes. Though the precise source of the light Zn added to the upper ocean remains an open question, it seems possible that it could be anthropogenic in origin.

Acknowledgements

We would like to thank the captain, the crew and the co-chief scientist Pascale Lherminier, for their great work and support during the GEOVIDE cruise. Special thanks go to members of the trace metal clean sampling team including Julia Boutorh, Marie Cheize, Leonardo Contreira, François Lacan, Jan-Lukas Menzel Barraqueta and Rachel Shelley. We also would like to thank Fabien Perault, Emmanuel De Saint Léger (CNRS DT-INSU) for their help during the CTD deployments; Catherine Schmechtig for the GEOVIDE database management; Emilie Grossteffan, Manon Le

Goff, Morgane Gallinari and Paul Tréguer (LEMAR, IUEM) for the analysis of nutrients. The GEOVIDE project was supported by the French National Research Agency (ANR-13-BS06-0014 and ANR-12-PDOC-0025-01), the French National Centre for Scientific Research (CNRS-LEFE-CYBER), Ifremer and the “Laboratoire d’Excellence” Labex-Mer (ANR-10-LABX-19). This work received financial support from the Swiss National Science Foundation through grant 200020_165904.

References

Achterberg, E.P., Steigenberger, S., Marsay, C.M., LeMoigne, F.A.C., Painter, S.C., Baker, A.R., Connelly, D.P., Moore, C.M., Tagliabue, A., Tanhua, T., 2018. Iron biogeochemistry in the high latitude North Atlantic Ocean. Sci. Rep. 8, 1–15. doi:10.1038/s41598-018-19472-1

Aminot, A., Kérouel, R., 2007. Dosage automatique des nutriments dans les eaux marines: méthodes en flux continu, Ifremer-Qu. ed.

Archer, C., Andersen, M.B., Cloquet, C., Conway, T.M., Dong, S., Ellwood, M., Moore, R., Nelson, J., Rehkämper, M., Rouxel, O., Samanta, M., Shin, K.C., Sohrin, Y., Takano, S., Wasylenki, L., 2017. Inter-calibration of a proposed new primary reference standard AA-ETH Zn for zinc isotopic analysis. J. Anal. At. Spectrom. 32, 415–419. doi:10.1039/c6ja00282j

Archer, C., Vance, D., Butler, I., 2004. Abiotic Zn isotope fractionations associated with ZnS precipitation. Geochim. Cosmochim. Acta 68, A325–A325. doi:10.1016/j.gca.2004.05.008

Bermin, J., Vance, D., Archer, C., Statham, P.J., 2006. The determination of the isotopic composition of Cu and Zn in seawater. Chem. Geol. 226, 280–297. doi:10.1016/j.chemgeo.2005.09.025

Bruland, K.W., 1980. Oceanographic distributions of cadmium, zinc, nickel, and copper in the North Pacific. Earth Planet. Sci. Lett. 47, 176–198. doi:10.1016/0012-821X(80)90035-7

Conway, T.M., Hamilton, D.S., Shelley, R.U., Aguilar-Islas, A.M., Landing, W.M., Mahowald, N.M., John, S.G., 2019. Tracing and constraining anthropogenic aerosol iron fluxes to the North Atlantic Ocean using iron isotopes. Nat. Commun. 10, 2628. doi:10.1038/s41467-019-10457-w

Conway, T.M., John, S.G., 2015. The cycling of iron, zinc and cadmium in the North East Pacific Ocean - Insights from stable isotopes. Geochim. Cosmochim. Acta 164, 262–283. doi:10.1016/j.gca.2015.05.023

Conway, T.M., John, S.G., 2014. The biogeochemical cycling of zinc and zinc isotopes in the North Atlantic Ocean. Global Biogeochem. Cycles 28, 1111–1128. doi:10.1002/2014GB004862.Received

Conway, T.M., Rosenberg, A.D., Adkins, J.F., John, S.G., 2013. A new method for precise determination of iron, zinc and cadmium stable isotope ratios in seawater by double-spike mass spectrometry. Anal. Chim. Acta 793, 44–52. doi:10.1016/j.aca.2013.07.025

Cotté-Krief, M.-H., Guieu, C., Thomas, A.J., Martin, J.-M., 2000. Sources of Cd, Cu, Ni and Zn in Portuguese coastal waters. Mar. Chem. 71, 199–214.

Cutter, G., Casciotti, K., Croot, P., Geibert, W., Heimbürger, L.-E., Lohan, M., Planquette, H., Van De Flierdt, T., 2017. Sampling and the sample-handling protocoles for GEOTRACES cruises. doi:http://www.geotraces.org/science/intercalibration/222-sampling-and-sample-handling-protocols-for-geotraces-cruises

Daniault, N., Mercier, H., Lherminier, P., Sarafanov, A., Falina, A., Zunino, P., Pérez, F.F., Ríos, A.F., Ferron, B., Huck, T., Thierry, V., Gladyshev, S., 2016. The northern North Atlantic Ocean mean circulation in the early 21st century. Prog. Oceanogr. 146, 142–158. doi:10.1016/j.pocean.2016.06.007

de Souza, G.F., Khatiwala, S.P., Hain, M.P., Little, S.H., Vance, D., 2018. On the origin of the marine zinc–silicon correlation. Earth Planet. Sci. Lett. 492, 22–34.

585 doi:10.1016/j.epsl.2018.03.050
586 de Souza, G.F., Reynolds, B.C., Rickli, J., Frank, M., Saito, M.A., Gerringa, L.J.A.,
587 Bourdon, B., 2012. Southern Ocean control of silicon stable isotope distribution
588 in the deep Atlantic Ocean. Global Biogeochem. Cycles 26, 1–13.
589 doi:10.1029/2011GB004141
590 de Souza, G.F., Slater, R.D., Hain, M.P., Brzezinski, M.A., Sarmiento, J.L., 2015.
591 Distal and proximal controls on the silicon stable isotope signature of North
592 Atlantic Deep Water. Earth Planet. Sci. Lett. 432, 342–353.
593 doi:10.1016/j.epsl.2015.10.025
594 Desboeufs, K. V., Sofikitis, A., Losno, R., Colin, J.L., Ausset, P., 2005. Dissolution
595 and solubility of trace metals from natural and anthropogenic aerosol particulate
596 matter. Chemosphere 58, 195–203. doi:10.1016/j.chemosphere.2004.02.025
597 Ellwood, M.J., Van den Berg, C.M.G., 2000. Zinc speciation in the northeastern
598 Atlantic ocean. Mar. Chem. 68, 295–306. doi:10.1016/S0304-4203(99)00085-7
599 Fekiacova, Z., Cornu, S., Pichat, S., 2015. Tracing contamination sources in soils
600 with Cu and Zn isotopic ratios. Sci. Total Environ. 517, 96–105.
601 doi:10.1016/j.scitotenv.2015.02.046
602 Fujii, T., Moynier, F., Pons, M.L., Albarède, F., 2011. The origin of Zn isotope
603 fractionation in sulfides. Geochim. Cosmochim. Acta 75, 7632–7643.
604 doi:10.1016/j.gca.2011.09.036
605 García-Ibáñez, M.I., Pérez, F.F., Lherminier, P., Zunino, P., Mercier, H., Tréguer, P.,
606 2018. Water mass distributions and transports for the 2014 GEOVIDE cruise in
607 the North Atlantic. Biogeosciences 15, 2075–2090. doi:10.5194/bg-15-2075-
608 2018
609 Gourain, A., Planquette, H., Cheize, M., Lemaitre, N., Menzel Barraqueta, J.L.,
610 Shelley, R., Lherminier, P., Planquette, H., 2019. Inputs and processes affecting
611 the distribution of particulate iron in the North Atlantic along the GEOVIDE
612 (GEOTRACES GA01) section. Biogeosciences 16, 1563–1582. doi:10.5194/bg-
613 16-1563-2019
614 Hsu, S.C., Lin, F.J., Jeng, W.L., 2005. Seawater solubility of natural and
615 anthropogenic metals within ambient aerosols collected from Taiwan coastal
616 sites. Atmos. Environ. 39, 3989–4001. doi:10.1016/j.atmosenv.2005.03.033
617 Jenkins, W.J., Smethie, W.M., Boyle, E.A., Cutter, G.A., 2015. Water mass analysis
618 for the U.S. GEOTRACES (GA03) North Atlantic sections. Deep. Res. Part II
619 Top. Stud. Oceanogr. 116, 6–20. doi:10.1016/j.dsr2.2014.11.018
620 John, S.G., Conway, T.M., 2014. A role for scavenging in the marine biogeochemical
621 cycling of zinc and zinc isotopes. Earth Planet. Sci. Lett. 394, 159–167.
622 doi:10.1016/j.epsl.2014.02.053
623 John, S.G., Geis, R.W., Saito, M.A., Boyle, E.A., 2007. Zinc isotope fractionation
624 during high-affinity and low-affinity zinc transport by the marine diatom
625 Thalassiosira oceanica. Limnol. Oceanogr. 52, 2710–2714.
626 doi:10.4319/lo.2007.52.6.2710
627 John, S.G., Helgoe, J., Townsend, E., 2018. Biogeochemical cycling of Zn and Cd
628 and their stable isotopes in the Eastern Tropical South Pacific. Mar. Chem. 201,
629 66–76. doi:10.1016/j.marchem.2017.06.003
630 John, S.G., Rouxel, O.J., Craddock, P.R., Engwall, A.M., Boyle, E.A., 2008. Zinc
631 stable isotopes in seafloor hydrothermal vent fluids and chimneys. Earth Planet.
632 Sci. Lett. 269, 17–28. doi:10.1016/j.epsl.2007.12.011
633 Kim, T., Obata, H., Nishioka, J., Gamo, T., 2017. Distribution of Dissolved Zinc in the
634 Western and Central Subarctic North Pacific. Global Biogeochem. Cycles 31,

635 1454–1468. doi:10.1002/2017GB005711
636 Köbberich, M., Vance, D., 2019. Zn isotope fractionation during uptake into marine
637 phytoplankton: Implications for oceanic zinc isotopes. Chem. Geol.
638 doi:10.1016/j.chemgeo.2019.04.004
639 Le Gall, A.C., Statham, P.J., Morley, N.J., Hydes, D.J., Hunt, C.H., 1999. Processes
640 influencing distributions and concentrations of Cd, Cu, Mn and Ni at the North
641 West European shelf break. Mar. Chem. 68, 97–115.
642 Le Roy, E., Sanial, V., Charette, M.A., van Beek, P., Lacan, F., Jacquet, S.H.M.,
643 Henderson, P.B., Souhaut, M., García-Ibáñez, M.I., Jeandel, C., Pérez, F.F.,
644 Sarthou, G., 2018. The 226Ra–Ba relationship in the North Atlantic during
645 GEOTRACES-GA01. Biogeosciences 15, 3027–3048. doi:10.5194/bg-15-3027-
646 2018
647 Liao, W.H., Takano, S., Yang, S.C., Huang, K.F., Sohrin, Y., Ho, T.Y., 2020. Zn
648 isotope composition in the water column of the northwestern Pacific ocean: the
649 importance of external sources. Global Biogeochem. Cycles 34.
650 doi:10.1029/2019GB006379
651 Little, S.H., Vance, D., Walker-Brown, C., Landing, W.M., 2014. The oceanic mass
652 balance of copper and zinc isotopes, investigated by analysis of their inputs, and
653 outputs to ferromanganese oxide sediments. Geochim. Cosmochim. Acta 125,
654 673–693. doi:10.1016/j.gca.2013.07.046
655 Longhurst, A.R., 2010. Ecological geography of the sea, Academic P. ed. San Diego.
656 Marshall, J., Speer, K., 2012. Closure of the meridional overturning circulation
657 through Southern Ocean upwelling. Nat. Geosci. 5, 171–180.
658 doi:10.1038/ngeo1391
659 Mattielli, N., Petit, J.C.J., Deboudt, K., Flament, P., Perdrix, E., Taillez, A., Rimetz-
660 Planchon, J., Weis, D., 2009. Zn isotope study of atmospheric emissions and
661 dry depositions within a 5 km radius of a Pb-Zn refinery. Atmos. Environ. 43,
662 1265–1272. doi:10.1016/j.atmosenv.2008.11.030
663 Middag, R., de Baar, H.J.W., Bruland, K.W., 2019. The relationships between
664 dissolved zinc and major nutrients phosphate and silicate along the
665 GEOTRACES GA02 transect in the west Atlantic Ocean. Global Biogeochem.
666 Cycles 33, 63–84. doi:10.1029/2018GB006034
667 Morel, F.M.M., Price, N.M., 2003. The Biogeochemical Cycles of Trace Metals in the
668 Oceans. Science (80-.). 300, 944–947. doi:10.1126/science.1083545
669 Moynier, F., Vance, D., Fujii, T., Savage, P., 2017. The Isotope Geochemistry of Zinc
670 and Copper. Rev. Mineral. Geochemistry 82, 543–600.
671 doi:10.2138/rmg.2017.82.13
672 Ohnemus, D.C., Lam, P.J., 2014. Cycling of Lithogenic Marine Particulates in the US
673 GEOTRACES North Atlantic Transect. Deep Sea Res. Part II Top. Stud.
674 Oceanogr. 116, 283–302. doi:http://dx.doi.org/10.1016/j.dsr2.2014.11.019
675 Paillet, J., Arhan, M., McCartney, M.S., 1998. Spreading of Labrador Sea Water in
676 the eastern North Atlantic. J. Geophys. Res. Ocean. 103, 10223–10239.
677 doi:10.1029/98jc00262
678 Peel, K., Weiss, D., Sigg, L., 2009. Zinc isotope composition of settling particles as a
679 proxy for biogeochemical processes in lakes: Insights from the eutrophic Lake
680 Greifen, Switzerland. Limnol. Oceanogr. 54, 1699–1708.
681 doi:10.4319/lo.2009.54.5.1699
682 Roshan, S., DeVries, T., Wu, J., Chen, G., 2018. The Internal Cycling of Zinc in the
683 Ocean. Global Biogeochem. Cycles 32, 1833–1849.
684 doi:10.1029/2018GB006045

685 Roshan, S., Wu, J., 2015. Water mass mixing: The dominant control on the zinc
686 distribution in the North Atlantic Ocean. Global Biogeochem. Cycles 29, 1060–
687 1074. doi:10.1002/2014GB005026
688 Roshan, S., Wu, J., Jenkins, W.J., 2016. Long-range transport of hydrothermal
689 dissolved Zn in the tropical South Pacific. Mar. Chem. 183, 25–32.
690 doi:10.1016/j.marchem.2016.05.005
691 Samanta, M., Ellwood, M.J., Sinoir, M., Hassler, C.S., 2017. Dissolved zinc isotope
692 cycling in the Tasman Sea, SW Pacific Ocean. Mar. Chem. 192, 1–12.
693 doi:10.1016/j.marchem.2017.03.004
694 Samanta, M., Ellwood, M.J., Strzepek, R.F., 2018. Zinc isotope fractionation by
695 Emiliania huxleyi cultured across a range of free zinc ion concentrations. Limnol.
696 Oceanogr. 63, 660–671. doi:10.1002/lno.10658
697 Sarmiento, J.L., Gruber, N., Brzezinski, M. a, Dunne, J.P., 2004. High-latitude
698 controls of thermocline nutrients and low latitude biological productivity. Nature
699 427, 56–60. doi:10.1038/nature10605
700 Schlitzer, R., Anderson, R.F., Masferrer Dodas, E., Lohan, M.C., Geibert, W.,
701 Tagliabue, A., Bowie, A.R., Jeandel, C., Maldonado, M.T., Landing, W.M.,
702 Cockwell, D., Steinfeldt, R., Morton, P.L., Queroue, F., Hawco, N., Nishioka, J.,
703 Milne, A., Cossa, D., Pradoux, C., Schlitzer, R., Vivancos, S.M., Fleisher, M.Q.,
704 Bauch, D., Closset, I., van Aken, H.M., Daniels, C., Gerringa, L.J.A., Cullen,
705 J.T., Goldstein, S.L., van de Flierdt, T., Church, T.M., Dumousseaud, C.,
706 Bouman, H., Hatta, M., Barraqueta, J.-L.M., Slater, E., Swift, J.H., Little, S., Wu,
707 J., Till, R., van Heuven, S., Lherminier, P., Nakaguchi, Y., Agather, A., Remenyi,
708 T., Rigaud, S., Owens, S., Lam, P.J., Cardinal, D., Wyatt, N., Chance, R.,
709 Carlson, C., Bates, N.R., Andersen, M., Jenkins, W.J., Sigman, D.M., Hartman,
710 A., Kumamoto, Y., Kenna, T.C., Hathorne, E.C., Xie, R.C., Wuttig, K., Ziveri, P.,
711 Hayes, C.T., Butler, E., Salt, L.A., Tuerena, R., Croot, P., Dieu, H.T., Dodas,
712 E.M., Casacuberta, N., Townsend, A.T., Heimbürger, L.-E., Velazquez, S.,
713 Laan, P., Robinson, L.F., Thomas, A., Heller, M., Gault-Ringold, M., van
714 Weerlee, E., Till, C.P., Radic, A., Branellec, P., Ellwood, M., Rijkenberg, M.J.A.,
715 Lambelet, M., Isshiki, K., Speich, S., Garcia-Solsona, E., Rehkämper, M., Black,
716 E., Kipp, L., Niedermiller, J., Stichel, T., Fröllje, H., Resing, J.A., Gonzalez, S.R.,
717 Alexandra Weigand, M., Lee, J.-M., Cai, P., Chaves, J.E., Dulaquais, G.,
718 Brissebrat, G., Villa-Alfageme, M., Warner, M.J., Shelley, R., Weinstein, Y.,
719 Moncoiffe, G., Cockwell, D., Abadie, C., Wu, Y., Ho, P., Stirling, C.H., Tagliabue,
720 A., Echegoyen-Sanz, Y., Mieruch, S., Schlosser, C., Sonke, J.E., Measures, C.,
721 van der Merwe, P., Mcclain, C.R., Rosenberg, M., Gilbert, M., Lohan, M.,
722 Castrillejo, M., Duggan, B., Bruland, K.W., Noble, A., Woodward, E.M.S.,
723 Townsend, E., Labatut, M., Sarthou, G., Auro, M., Schnetger, B., Helgoe, J.,
724 Galer, S.J.G., Bakker, K., Jacquot, J.E., Boye, M., Kretschmer, S., Obata, H.,
725 Xiang, Y., Fahrbach, E., Christl, M., Fripiat, F., Russell Flegal, A., Janssen, D.J.,
726 Middag, R., Planquette, H., Zieringer, M., Huang, K.-F., Scher, H., Roeske, T.,
727 Baars, O., Moffett, J.W., Paul, M., Vance, D., Nakayama, N., Hsieh, Y.-T.,
728 Rember, R., Colman, A., Mor, P.C., Bull, A., Ryabenko, E., Twining, B.S.,
729 Brzezinski, M., Sanial, V., O'Sullivan, J., Wisotzki, A., Masque, P., Rintoul, S.,
730 Conway, T.M., Lacan, F., Zhao, Y., Stewart, G., Lu, Y., Peters, B., Nishiuchi, A.,
731 Baker, A.R., Zurbrick, C., Lamborg, C.H., John, S., Behrens, M.K., Pahnke, K.,
732 Thorne, K., Schauer, U., Cheng, H., Achterberg, E.P., Rutgers van der Loeff,
733 M.M., Cutter, G.A., Kadko, D.C., Brumsack, H.-J., Dehairs, F., Semiletov, I., van
734 Beek, P., Snaith, H., van Ooijen, J., Klar, J.K., Grissom, K., Morris, P.J., Scott,

735 P., Friedrich, J., Aguliar-Islas, A., Rickli, J., Chamizo, E., Sherrell, R.M.,
736 Fitzsimmons, J.N., Ober, S., Charette, M.A., Boyd, P., Smethie, W.M., Watson,
737 R., Maldonado, M.T., Landing, W.M., Rolison, J.M., Hammerschmidt, C., Zhang,
738 P., Saito, M.A., Geibert, W., Rodellas, V., Slagter, H.A., Sohrin, Y., Deng, F.,
739 Roca-Martí, M., Kayser, R., Le Moigne, F.A.C., Zhang, J., Carrasco, G., López-
740 Lora, M., Kim, T., Roshan, S., Sohst, B., Jones, J.L., Zheng, X.-Y., Hassler,
741 C.S., George, E., Browning, T., Henderson, G.M., Bopp, L., Puigcorbé, V.,
742 Klunder, M., Buck, K.N., Ohnemus, D.C., Casciotti, K.L., Basak, C., Boyle, E.A.,
743 Mawji, E., Lechtenfeld, O.J., Anderson, R.F., Bown, J., Chever, F., Godoy, J.M.,
744 Gamo, T., Yoshikawa, H., Zunino, P., Zimmer, L.A., Horner, T.J., Mehic, S., de
745 Baar, H.J., Henderson, P.B., Planchon, F., Shiller, A.M., Sedwick, P.N.,
746 Ganeshram, R.S., Wake, B., Jones, E.M., Stutsman, J., Venchiarutti, C.,
747 Edwards, R.L., Minami, T., Humphreys, M.P., Bowie, A., Buesseler, K., Garcia-
748 Orellana, J., Schallenberg, C., Abouchami, W., Moore, W.S., Pavia, F., Singh,
749 S.K., Baskaran, M., Zheng, L., Jeandel, C., Weiss, D., Le Roy, E., Bluhm, K.,
750 Bowman, K., Swarr, G.J., Rauschenberg, S., Khondoker, R., Pena, L.D., Frank,
751 M., Quay, P., Bridgestock, L., Voelker, A.H.L., Archer, C., Xue, Z., Buck, C.S.,
752 2018. The GEOTRACES Intermediate Data Product 2017. Chem. Geol. 493,
753 210–223. doi:10.1016/j.chemgeo.2018.05.040
754 Shelley, R.U., Landing, W.M., Ussher, S.J., Planquett, H., Sarthou, G., 2018.
755 Regional trends in the fractional solubility of Fe and other metals from North
756 Atlantic aerosols (GEOTRACES GA01 and GA03) following a two-stage leach.
757 Biogeosciences 1–31. doi:10.5194/bg-2017-415
758 Shelley, R.U., Roca-Martí, M., Castrillejo, M., Masqué, P., Landing, W.M.,
759 Planquette, H., Sarthou, G., 2017. Quantification of trace element atmospheric
760 deposition fluxes to the Atlantic Ocean (>40°N; GEOVIDE, GEOTRACES GA01)
761 during spring 2014. Deep. Res. Part I Oceanogr. Res. Pap. 119, 34–49.
762 doi:10.1016/j.dsr.2016.11.010
763 Sieber, M., Conway, T.M., de Souza, G.F., Hassler, C.S., Ellwood, M.J., Vance, D.,
764 2020. Cycling of zinc and its isotopes across multiple zones of the Southern
765 Ocean: Insights from the Antarctic Circumnavigation Expedition. Geochim.
766 Cosmochim. Acta 268, 310–324. doi:10.1016/j.gca.2019.09.039
767 Siebert, C., Nägler, T.F., Kramers, J.D., 2001. Determination of molybdenum isotope
768 fractionation by double-spike multicollector inductively coupled plasma mass
769 spectrometry. Geochemistry, Geophys. Geosystems 2.
770 doi:10.1029/2000GC000124
771 Sunda, W., 1989. Trace metal interactions with marine phytoplankton. Biol.
772 Oceanogr. 6, 411–442. doi:10.1080/01965581.1988.10749543
773 Sutton, J.N., de Souza, G.F., García-Ibáñez, M.I., Rocha, C.L.D. La, 2018. The
774 silicon stable isotope distribution along the GEOVIDE section (GEOTRACES
775 GA-01) of the North Atlantic Ocean. Biogeosciences 15, 5663–5676.
776 doi:10.5194/bg-15-5663-2018
777 Takano, S., Tanimizu, M., Hirata, T., Sohrin, Y., 2013. Determination of isotopic
778 composition of dissolved copper in seawater by multi-collector inductively
779 coupled plasma mass spectrometry after pre-concentration using an
780 ethylenediaminetriacetic acid chelating resin. Anal. Chim. Acta 784, 33–41.
781 doi:10.1016/j.aca.2013.04.032
782 Tonnard, M., Planquette, H., Bowie, A.R., van der Merwe, P., Gallinari, M., Desprez
783 de Gésincourt, F., Germain, Y., Gourain, A., Benetti, M., Reverdin, G., Tréguer,
784 P., Boutorh, J., Cheize, M., Menzel Barraqueta, J.-L., Pereira-Contreira, L.,

Shelley, R., Lherminier, P., Sarthou, G., 2020. Dissolved iron in the North Atlantic Ocean and Labrador Sea along the GEOVIDE section (GEOTRACES section GA01). Biogeosciences 14, 917–943. doi:10.5194/bg-17-917-2020

van Aken, H.M., Becker, G., 1996. Hydrography and through-flow in the north-eastern North Atlantic Ocean: The NANSEN project. Prog. Oceanogr. 38, 297–346. doi:10.1016/S0079-6611(97)00005-0

Vance, D., de Souza, G.F., Zhao, Y., Cullen, J.T., Lohan, M.C., 2019. The relationship between zinc, its isotopes, and the major nutrients in the North-East Pacific. Earth Planet. Sci. Lett. 525. doi:10.1016/j.epsl.2019.115748

Vance, D., Little, S.H., Archer, C., Cameron, V., Andersen, M.B., Rijkenberg, M.J.A., Lyons, T.W., 2016. The oceanic budgets of nickel and zinc isotopes: the importance of sulfidic environments as illustrated by the Black Sea. Philos. Trans. R. Soc. A 374. doi:10.1098/rsta.2015.0294

Vance, D., Little, S.H., de Souza, G.F., Khatiwala, S., Lohan, M.C., Middag, R., 2017. Silicon and zinc biogeochemical cycles coupled through the Southern Ocean. Nat. Geosci. 1–6. doi:10.1038/ngeo2890

Wang, R.M., Archer, C., Bowie, A.R., Vance, D., 2019. Zinc and nickel isotopes in seawater from the Indian Sector of the Southern Ocean: The impact of natural iron fertilization versus Southern Ocean hydrography and biogeochemistry. Chem. Geol. 511, 452–464. doi:10.1016/j.chemgeo.2018.09.010

Weber, T., John, S., Tagliabue, A., DeVries, T., 2018. Biological uptake and reversible scavenging of zinc in the global ocean. Science (80-.). 361, 72–76. doi:10.1126/science.aap8532

Wheat, C.G., Mottl, M.J., Rudnicki, M., 2002. Trace element and REE composition of a low-temperature ridge-flank hydrothermal spring. Geochim. Cosmochim. Acta 66, 3693–3705. doi:10.1016/S0016-7037(02)00894-3

Williams, R.G., Roussenov, V., Follows, M.J., 2006. Nutrient streams and their induction into the mixed layer. Global Biogeochem. Cycles 20, 1–18. doi:10.1029/2005GB002586

Wyatt, N.J., Milne, A., Woodward, E.M.S., Rees, A.P., Browning, T.J., Bouman, H.A., Worsfold, P.J., Lohan, M.C., 2014. Biogeochemical cycling of dissolved zinc along the GEOTRACES South Atlantic transect GA10 at 40°S. Global Biogeochem. Cycles 28, 44–56. doi:10.1002/2013GB004637

Zhao, Y., Vance, D., Abouchami, W., de Baar, H.J.W., 2014. Biogeochemical cycling of zinc and its isotopes in the Southern Ocean. Geochim. Cosmochim. Acta 125, 653–672. doi:10.1016/j.gca.2013.07.045

Zurbrick, C.M., Boyle, E.A., Kayser, R.J., Reuer, M.K., Wu, J., Planquette, H., Shelley, R., Boutorh, J., Cheize, M., Contreira, L., Barraqueta, J.L.M., Lacan, F., Sarthou, G., 2018. Dissolved Pb and Pb isotopes in the North Atlantic from the GEOVIDE transect (GEOTRACES GA-01) and their decadal evolution. Biogeosciences 15, 4995–5014. doi:10.5194/bg-15-4995-2018

Figure 1

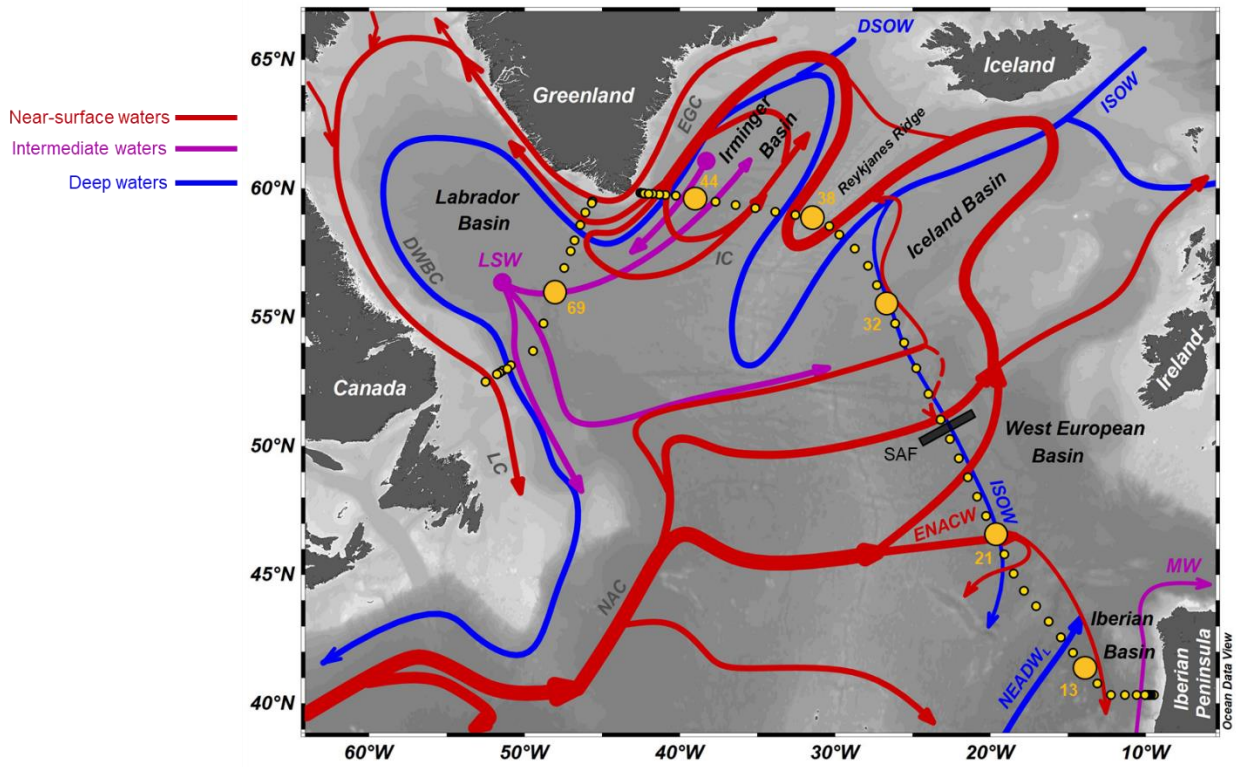

Figure 1: *Schematic diagram of the large scale circulation in the North Atlantic, adapted from García-Ibáñez et al., (2018). Abbreviations for the main hydrographic features indicated are as follows: Denmark Strait Overflow Water (DSOW), Iceland-Scotland Overflow Water (ISOW), Labrador Sea Water (LSW), Mediterranean Water (MW), North East Atlantic Deep Water lower (NEADW$_L$), East North Atlantic Central Water (ENACW), Labrador Current (LC), East Greenland Current (EGC), Irminger Current (IC) and the North Atlantic Current (NAC), Subarctic front (SAF). Yellow circles mark all stations sampled during GEOVIDE, with the large symbols representing the stations discussed in this study.*

Figure 2

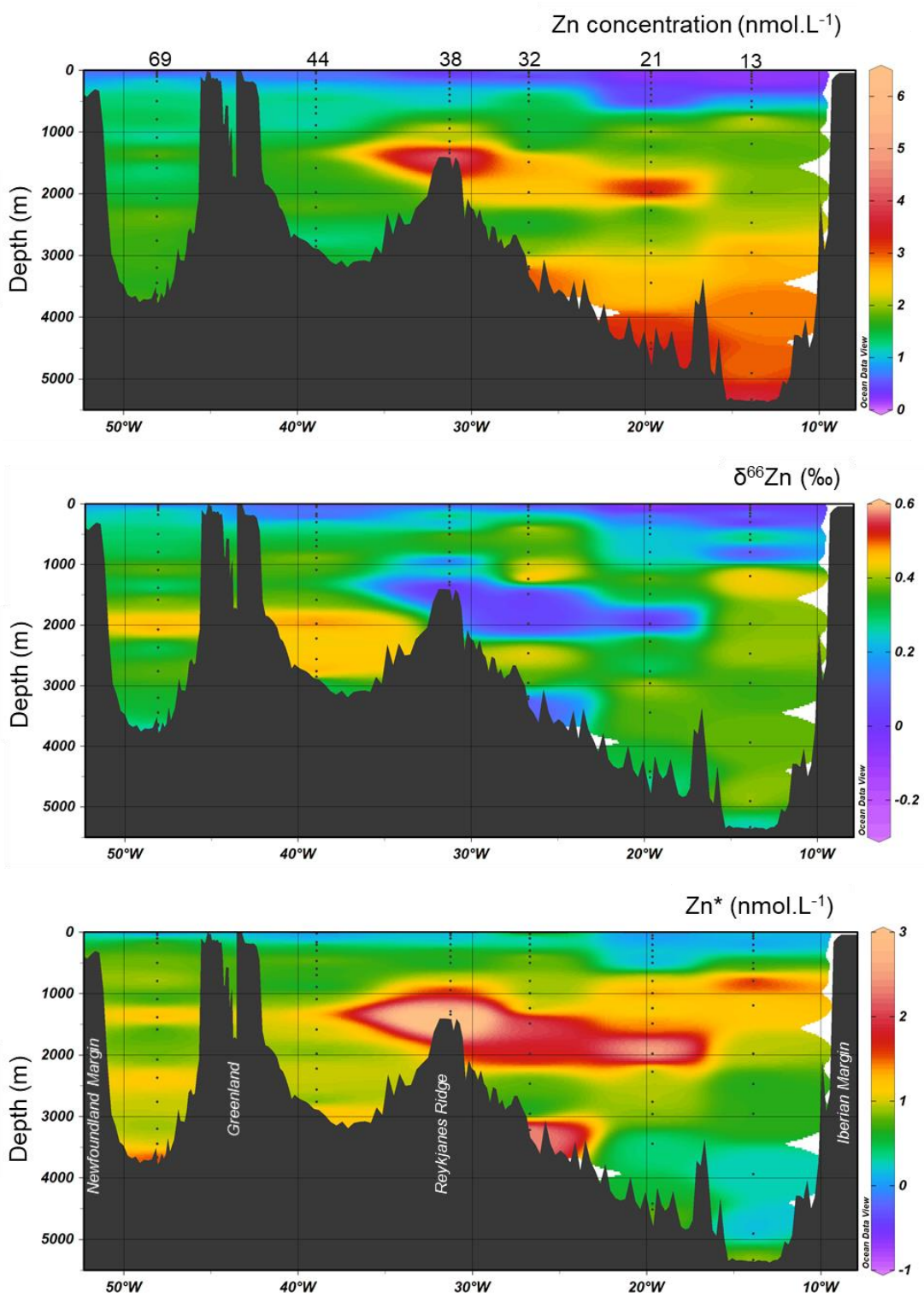

Figure 2: *Zn concentrations, Zn stable isotope composition ($\delta^{66}Zn$) and Zn* along the GEOVIDE transect. Black dots represent sample locations. Station numbers are indicated at the top of the Zn concentration section.*

Figure 3

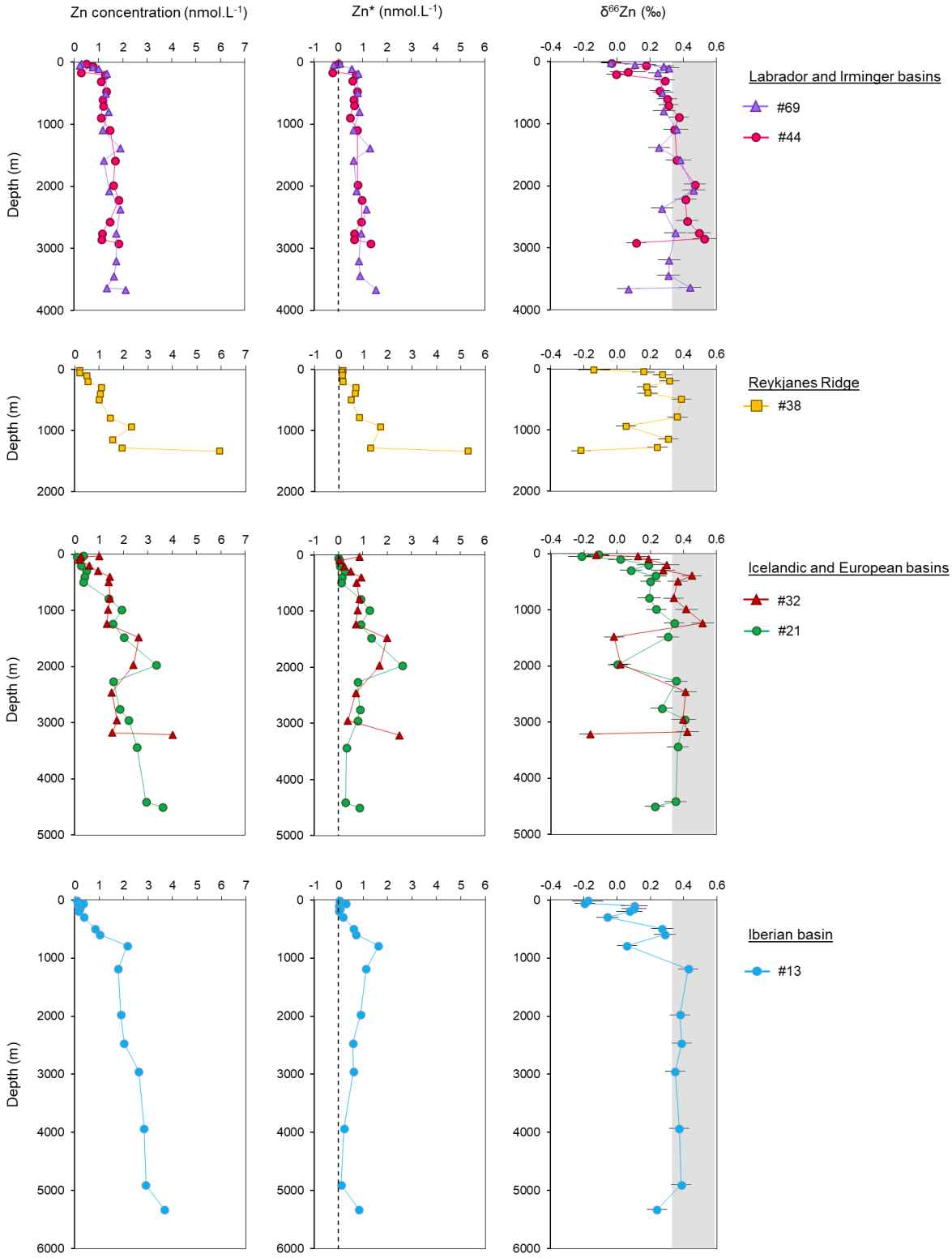

Figure 3: *Zn concentrations, Zn* and $\delta^{66}Zn$ signatures for the stations of the GEOVIDE transect. The shaded grey band shows the average $\delta^{66}Zn$ in the deep ocean.*

Figure 4

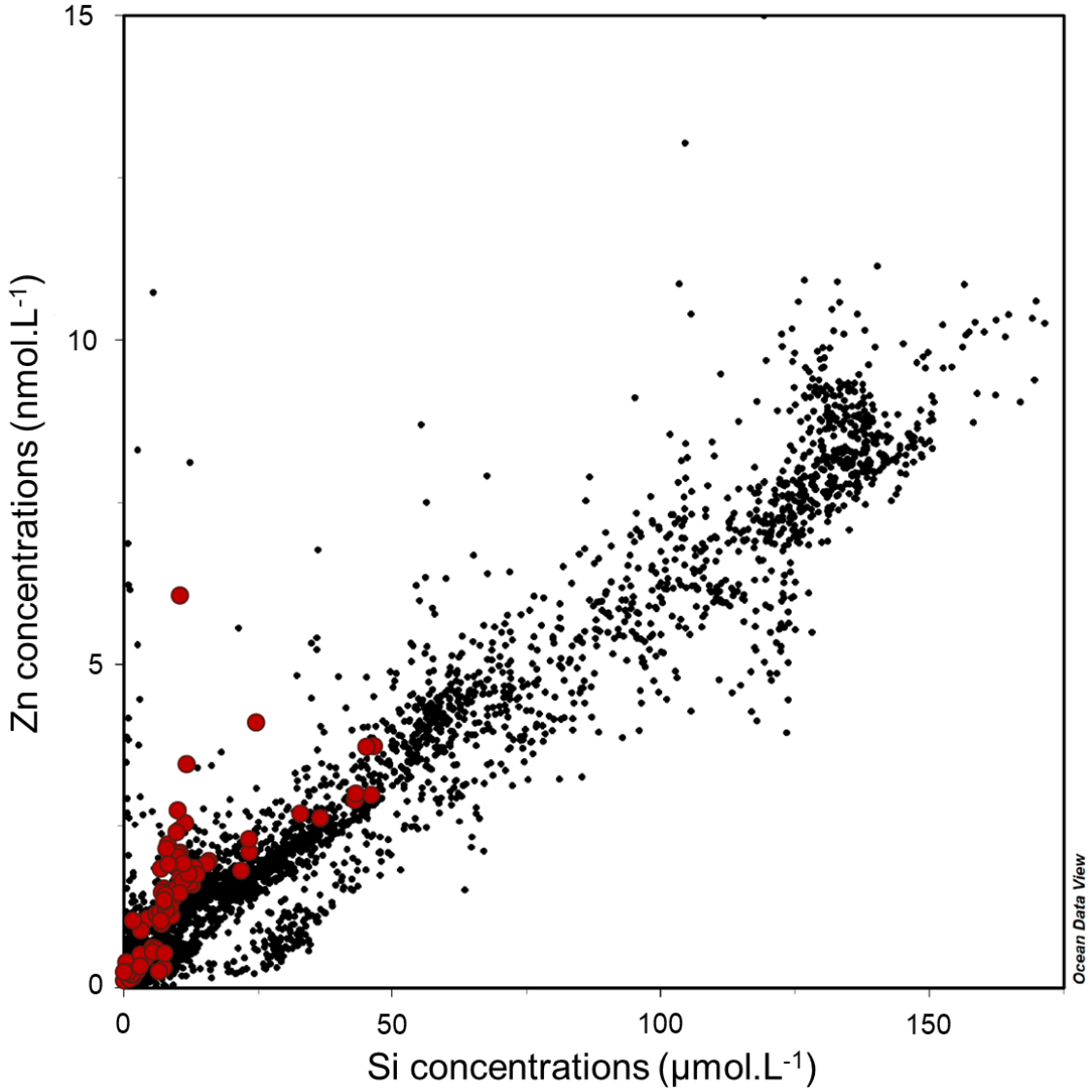

Figure 4: *Zinc concentrations plotted versus Si concentrations for all samples in the GEOTRACES IDP 2017 (Schlitzer et al., 2018; black dots), with our data from GEOVIDE in red.*

Figure 5

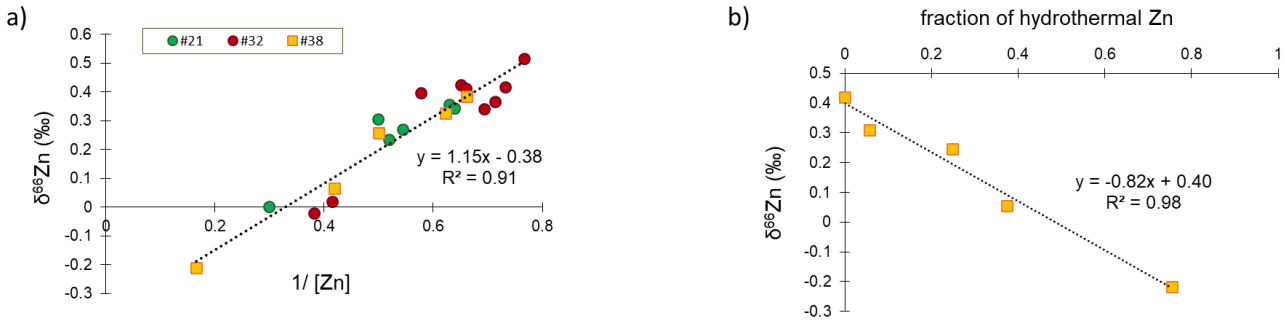

Figure 5: *a) Zinc isotope composition ($\delta^{66}Zn$) plotted against 1 / [Zn] at depths between 1337m (deepest data point) and 700m at Station 38, and between 3000m and 700m for Stations 21 and 32. b) Zinc isotope composition as a function of the fraction of hydrothermal Zn (see explanations in the text) for all samples at Station 38 that are influenced by the hydrothermal vent, and for background deep seawater (x = 0). The linear correlation provides an estimate of the isotope composition of a hydrothermal end-member when x =1 ($\delta^{66}Zn$ = -0.42 ‰).*

Figure 6

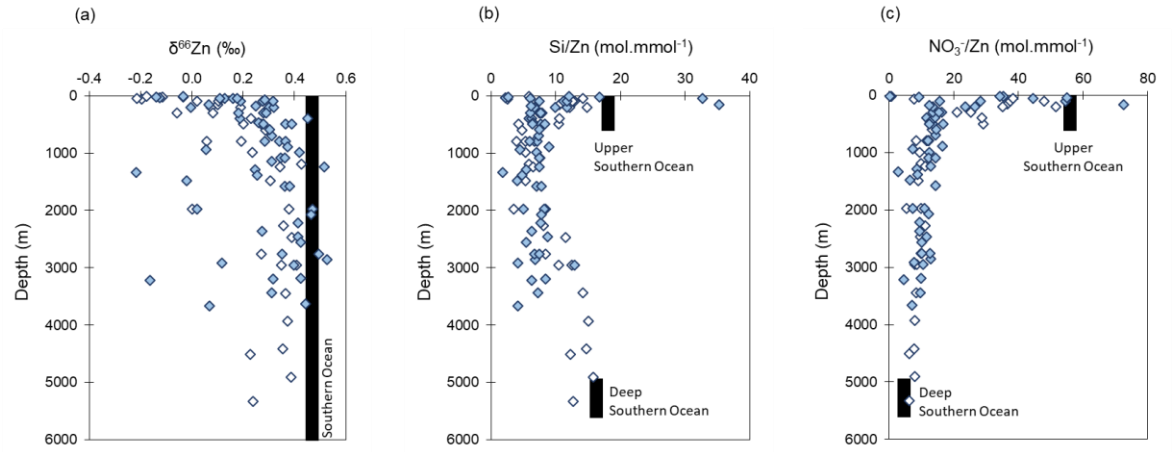

Figure 6: *Depth distribution of (a) $\delta^{66}Zn$, (b) Si/Zn and (c) NO_3^-/Zn ratios for the GEOVIDE stations 13 and 21 east of the Reykjanes Ridge, where abyssal waters of Southern Ocean origin dominate the deep ocean below 3000m (empty symbols) and for the GEOVIDE stations 32, 38, 44 and 69 (blue symbols). The black rectangles show the average $\delta^{66}Zn$, Si/Zn and NO_3^-/Zn ratios of the upper and deep Southern Ocean. While the deep North Atlantic has Zn isotope compositions and macronutrient/Zn ratios that are very close to the ultimate source of these water masses in the Southern Ocean, the upper ocean shows low Si/Zn, low NO_3^-/Zn and light Zn isotopes that are most consistent with a source of isotopically light Zn.*

Figure 7

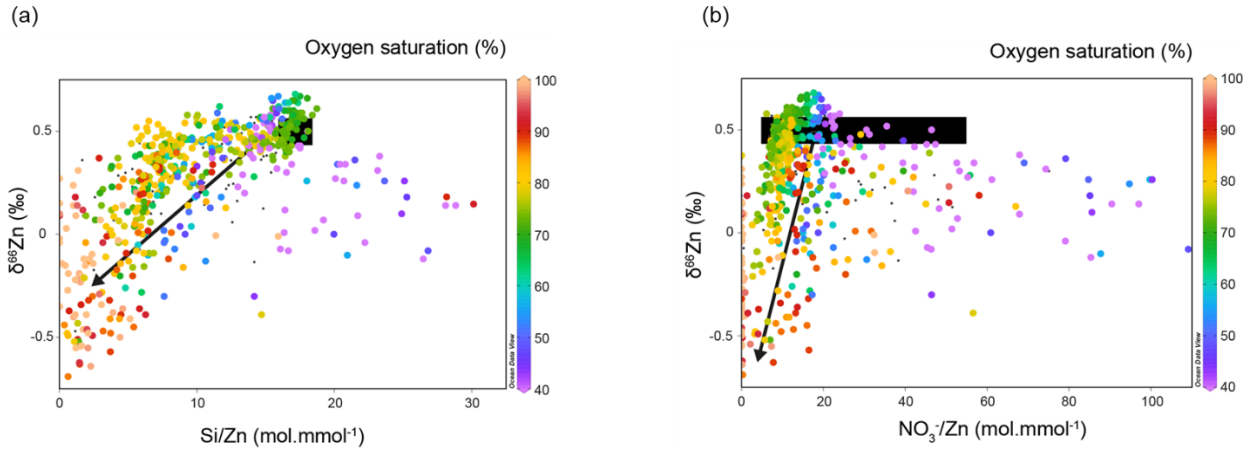

Figure 7: *$\delta^{66}Zn$ plotted against (a) Si/Zn and (b) NO_3^-/Zn ratios for the North Atlantic (GEOVIDE and GA03 cruises; this study and Conway and John, 2014). Data are colour-coded for oxygen saturation. The black rectangles show the average $\delta^{66}Zn$ and concentration ratios for the Southern Ocean. Black arrows indicate addition of isotopically light Zn relative to major nutrient. The intercepts of the black arrows, at NO_3^-/Zn and Si/Zn = 0 constrain the source of added Zn to have a $\delta^{66}Zn$ of around -0.5 ‰.*

Figure 8

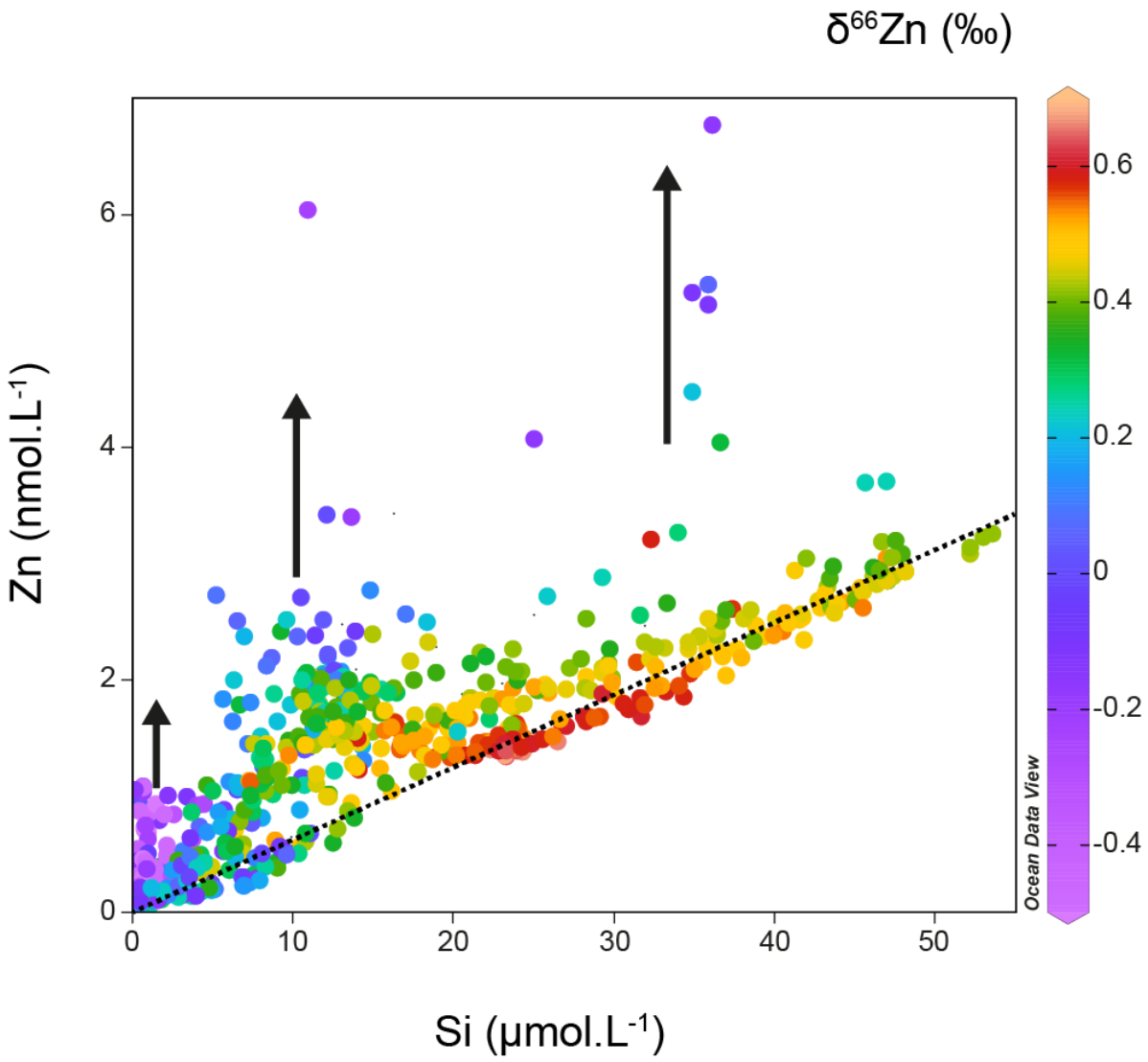

Figure 8: *Zinc concentrations against Si concentrations, with colours indicating Zn isotope composition, for the entire North Atlantic (GEOVIDE and GA03 cruises; this study and Conway and John, 2014). Black arrows indicate additions of Zn relative to Si. The dotted line represents the global Zn-Si relationship (GEOTRACES IDP 2017).*